

Minimum void length scale control in level set topology optimization subject to machining radii



Jikai Liu, Huangchao Yu, Yongsheng Ma*

Department of Mechanical Engineering, University of Alberta, Edmonton, AB, Canada

ARTICLE INFO

Article history:

Received 30 May 2016

Accepted 20 September 2016

Keywords:

Length scale control

Level set

Topology optimization

Machinability

ABSTRACT

This paper presents a minimum void length scale control method for structural topology optimization. Void length scale control has been actively investigated for decades, which intends to ensure the topology design manufacturable given the machining tool access. However, only a single lower bound has been applied in existing methods, which does not fit the multi-stage rough-to-finish machining. To fix this issue, the proposed minimum void length scale control method employs double lower bounds which corresponds to the rough and finish machining operations, respectively. This method has been implemented under the level set framework. For technical details, the rough machining lower bound is satisfied by developing a signed distance-related constraint, which ensures enough *space* for the rough machining tool movement and thus, guarantees the machining efficiency. The finish machining lower bound is addressed through the *curvature* flow control, which ensures the small features manufacturable and also a good finish dimension and surface. Through a few numerical case studies, it is proven that the minimum void length scale can be effectively controlled without sacrificing much of the structural performance.

© 2016 Elsevier Ltd. All rights reserved.

1. Introduction

Topology optimization has been actively investigated in the past few decades, which is now a major structural design methodology. Compared to trial and errors, topology optimization employs the automatic sensitivity-driven design loops which ensures outstanding efficiency and optimality; in addition, the method does not require much about the initial guess to produce creative design solutions, which makes it widely accepted by the design community.

Currently, SIMP (Solid Isotropic Material with Penalization) [1], ESO (Evolutionary Structural Optimization) [2], and level set [3,4] are the main topology optimization methods. These methods all have their unique characteristics and at the same time, are tightly associated. A broad range of design problems governed by different physical disciplines have been solved through these methods, i.e. solid mechanics [1–6], fluid dynamics [7,8], and thermal dynamics [9–11], etc. A few comprehensive literature surveys can be found in [12–14].

On the other hand, topology optimization is still poorly developed given certain engineering backgrounds. A critical

challenge is the manufacturability. In the past two decades, quite a few research publications have been dedicated to addressing this challenge. Length scale control is concerned for machining parts, which has been addressed based on both SIMP [15–24] and level set [25–30]; No interior void and undercut restrictions are necessary for injection molding/casting parts, which have also been addressed based on SIMP [31–36] and level set [37–39]; recently, manufacturability of 3D printed parts has also attracted plenty of concerns [40–43].

In this work, we focus on the length scale control of machining parts. As mentioned in the last paragraph, length scale control has been realized through both SIMP and level set. For SIMP, both the void and solid phases have been effectively controlled about the maximum and minimum length scales. For level set, the length scale control has been mainly implemented on the solid phase, but not the void, even though it is technically realizable. On the other hand, the existing minimum void length scale control methods only employ one lower bound, while in practice, the machining process is conducted from rough-to-finish by utilizing several machining tools. Therefore, a better method is needed which employs multiple lower bounds corresponding to the different-sized machining tools. Hence, a major contribution of this paper is the minimum void length scale control subject to multiple lower bounds, and this research is conducted under the level set framework.

* Corresponding author.

E-mail address: yongsheng.ma@ualberta.ca (Y. Ma).

2. Literature survey

Length scale control has been a long-lasting and challenging research problem which intends to guarantee the topology design manufacturable. To be specific, the void length scale should be larger than the minimum machining tool size, and the component length scale should not be too small because of the induced machining difficulties.

The pioneering works were the filtering method [44] and the local gradient constraint method [45], which were developed to eliminate the checker-board patterns and mesh dependency [46], while they marginally served to constrain the minimum length scale.

Dedicated to length scale control, Guest et al. [17] developed the Heaviside projection method, which projected the nodal densities into the element density field, and the minimum length scale was embedded in the projection operator. This method was effective in controlling the minimum component length scale, while the voids were not considered. Later, a modified double-projection was developed to restrict the minimum length scales of both phases [15]. Sigmund [21] developed a series of morphology-based density filters which realized both the single-phase and double-phase minimum length scale controls. However, as mentioned in the same paper, the sensitivity analysis cost of the double-phase minimum length scale control is overweighed. Based on the erode and dilate operations, a robust topology optimization method [19,20,22] was developed, in which multiple design realizations were evaluated while the worst case was optimized. The double-phase minimum length scale control can be achieved in case that the multiple realizations keep a consistent topology [19,22,24]. A drawback of this method is that multiple finite element analyses are required in each optimization loop.

Other than the density filters, length scale control has also been realized by adding constraints. Poulsen [18] developed the MOLE (MONotonicity based minimum LENGTH scale) method which utilized local integral constraints to check the monotonic density variations. The minimum length scale was explicitly satisfied for both phases by addressing these local integral constraints. Zuo et al. [47] utilized a minimum hole size constraint to remove the small hole features from the topology design. Guest et al. [16] realized the maximum component length scale control by adding constraints to restrict any circular area in diameter of the maximum length scale not fully filled. More recently, Zhang et al. [23] realized the simultaneous maximum and minimum component length scale controls through the structural skeleton based constraints.

Level set method is also effective in length scale control, and in some aspects, it has demonstrated superior characteristics. Chen et al. [26] and Luo et al. [29] employed a quadratic energy functional as part of the objective function, which successfully realized the strip-like topology design with controlled thickness. Liu et al. [28] developed a simplified thickness control functional to realize the close-to-constant rib thickness. Guo et al. [27] realized the concurrent maximum and minimum component length controls through the structural skeleton based constraints which are principally similar to [23]. The signed distance information facilitated the narrow-band structural skeleton extraction and related global constraints were constructed to restrict component length scales. Xia and Shi [30] modified the structural skeleton based method. The trimmed structural skeleton and the concept of maximal inscribable ball were employed to evaluate the length scale. Discrete point-based structural skeleton was extracted instead of a narrow band which facilitated the distance evaluation from skeleton. In this way, the length scale constraints were directly applied to the structural boundary points. Allaire et al. [25] explored the length scale control in depth under different

schemes of maximum length scale only, minimum length scale only, and the simultaneous control; additionally, a comparative discussion between thickness control functional and constraints was provided. Very recently, Wang et al. [48] realized the component length scale control through proposing and addressing the contour-offset based constraints.

Literature surveys about the length scale control can be found in [49,50].

In summary, diversified length scale control methods have been developed subject to different length scale control scenarios. However, these methods are only loosely connected to the engineering background of machining. In practice, a part is generally manufactured through multiple machining operations from rough-to-finish subject to different machining tool radii. Hence, multiple lower bounds of the minimum void length scale should be applied to ensure all the rough-to-finish machining operations executable, through which the machining efficiency and quality can be concurrently addressed. To the best of the authors' knowledge, the multiple lower bounds of the minimum void length scale have never been addressed, which is the main motivation of this research.

3. Void length scale control

3.1. Basic introduction to level set function

Level set function, $\Phi(\mathbf{X}) : R^n \mapsto R$, represents any structure in the implicit form, as:

$$\begin{cases} \Phi(\mathbf{X}) > 0, & \mathbf{X} \in \Omega / \partial\Omega \\ \Phi(\mathbf{X}) = 0, & \mathbf{X} \in \partial\Omega \\ \Phi(\mathbf{X}) < 0, & \mathbf{X} \in D / \Omega \end{cases} \quad (1)$$

where Ω represents the material domain, D indicates the entire design domain, and thus D/Ω represents the void.

Generally, the level set field satisfies the signed distance regulation through solution of Eq. (2), through which absolute of the level set value at any point represents its shortest distance to the structural boundary and the sign indicates the point to be either solid (>0), or void (<0).

$$|\nabla\Phi(\mathbf{X})| = 1. \quad (2)$$

Because of this signed distance characteristic, level set method was previously applied to tool path planning [51,52] for contour machining.

3.2. Void length scale control

As discussed earlier, the motivation of this work is to realize the minimum void length scale control subject to multiple lower bounds, which better fits the practical multi-stage machining process. Two new types of constraints have been proposed to achieve the goal, instead of the recently-popular structural skeleton based constraints [27,30].

Before presenting the details, a few characteristics of the void length scale control are discussed below.

(1) For load-bearing parts, the optimized material distribution generally follows strip-like shapes, while voids do not have regulated shape patterns.

(2) Given the machining background, it is not required to control the maximum void length scale. For minimum void length scale control, multiple lower bounds are required which correspond to the different machining tool radii, because a machining process generally includes several machining tool switches. It is worth noting that, for the sake of simplicity, two lower bounds are assumed in this work, in which the big one corresponds to the rough machining while the small one relates to the finish machining.

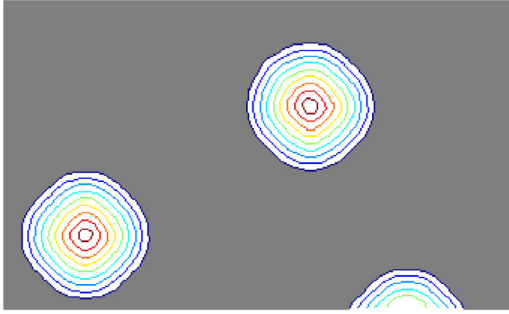


Fig. 1. Interior voids and a boundary void.

(3) The voids are categorized into two types: the interior void and the boundary void; see Fig. 1. Given the machining tool access, the interior voids will be applied of both lower bounds, while the boundary voids will only be constrained by the finish machining lower bound, because they are open voids which generally do not have tool access difficulty.

For the symbols, we define the i th interior void as Ω^v_i and its boundary as $\partial\Omega^v_i$. Peak point of the i th interior void is represented by P^v_i , which is defined as: $\{\mathbf{X} = \mathbf{X}(P^v_i) | \Phi(\mathbf{X}) < \Phi(\mathbf{X}^*)$, for any $\mathbf{X} \in \Omega^v_i\}$. The j th boundary void is represented by Ω^{bv}_j and its boundary by $\partial\Omega^{bv}_j$. As discussed earlier, two lower bounds are utilized for the void length scale, which are $0 < K_1 < K_2$. They are determined by $K_1 = R_1$ and $K_2 = kR_2$, where R_1 and R_2 are the machining tool radii for finish machining and rough machining, respectively. $k > 1$ is a positive number because there should be enough space for the rough machining tool movement.

So far, the assumptions and the symbolic representations have been introduced. Technical specifications will be presented in the rest of this section.

For any interior void, the lower bound K_1 is satisfied through adding the curvature-related constraint as demonstrated in Eq. (3).

$$-\frac{1}{K_1} < \kappa(\mathbf{X}) \leq 0, \quad \text{for any } \mathbf{X} \in \partial\Omega^v_i \text{ and } i = 1, 2, \dots, n \quad (3)$$

where κ means the curvature and n represents the number of interior voids.

Then, the lower bound K_2 is satisfied through adding the signed distance-related constraint as demonstrated in Eq. (4).

$$\Phi(P^v_i) \leq -K_2, \quad i = 1, 2, \dots, n. \quad (4)$$

This constraint is trivial in understanding that the level set value of the peak point indicates the interior void size.

As discussed earlier, the boundary voids will only be partially constrained by the finish machining lower bound K_1 , as presented in Eq. (5).

$$-\frac{1}{K_1} < \kappa(\mathbf{X}), \quad \text{for any } \mathbf{X} \in \partial\Omega^{bv}_j \text{ and } j = 1, 2, \dots, m \quad (5)$$

where m represents the number of boundary voids.

3.3. Identification of interior voids

As indicated by Eq. (4), level set value at the peak point reflects the interior void size, and therefore, it is important to properly identify the peak points. Therefore, the quick two-dimensional search is conducted and the peak points should satisfy the constraints in Eq. (6).

$$\begin{cases} \Phi_{k,l} - \Phi_{k-1,l} \leq 0 \\ \Phi_{k,l} - \Phi_{k+1,l} \leq 0 \\ \Phi_{k,l} - \Phi_{k,l-1} \leq 0 \\ \Phi_{k,l} - \Phi_{k,l+1} \leq 0. \end{cases} \quad (6)$$

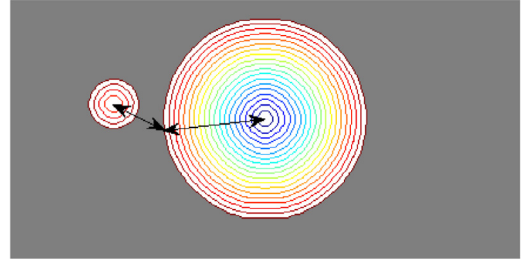


Fig. 2. Incorrect mapping based on the distance standard.



Fig. 3. The Michell structure problem (100 * 50).

Two situations may be identified: the peak point P^v_i is located inside the design domain or at the boundary. Only the former indicates the peak point of an interior void; the latter means the peak point of a boundary void, which is meaningless because not rough machining lower bound is applied to the boundary voids.

The other job is to identify the mapping relationship between the peak points and the related boundary points, because the peak point and the boundary points belonging to the same void should be clustered to facilitate the later sensitivity analysis. The distance would be a direct measure, because any boundary point and its closest peak point generally belong to the same void. However, directly applying the distance measure would cause mapping errors; see Fig. 2.

To fix this problem, a directional distance measure is proposed, as demonstrated in Eq. (7).

$$\begin{aligned} & \text{for any boundary point } \mathbf{X} \\ & \text{find the peak point } P^v_i, \text{ which satisfies:} \\ & \min . f \cdot |\mathbf{X}(P^v_i) - \mathbf{X}|, \quad i = 1, 2, \dots \\ & \begin{cases} f = 1, & \text{if } (\mathbf{X}(P^v_i) - \mathbf{X}) \cdot \mathbf{n}(\mathbf{X}) > 0 \\ f = +\infty, & \text{if } (\mathbf{X}(P^v_i) - \mathbf{X}) \cdot \mathbf{n}(\mathbf{X}) \leq 0 \end{cases} \quad (7) \\ & \mathbf{n}(\mathbf{X}) = -\frac{\nabla\Phi(\mathbf{X})}{|\nabla\Phi(\mathbf{X})|}. \end{aligned}$$

Through Eq. (7), a correct mapping can be established in case that the voids do not employ very irregular shapes. The boundary curvature constraints in Eqs. (3) and (5) can prevent the irregular-shape voids from appearing. In addition, a small batch of mis-mapping would not affect the overall convergence.

So far, the overall void length scale control method has been well established and its embedment into the optimization algorithm will be discussed in Section 4.

4. Optimization problem and its solution

A typical compliance minimization topology optimization problem including the void length scale constraints is formulated in Eq. (8). The structural compliance is to be minimized subject to

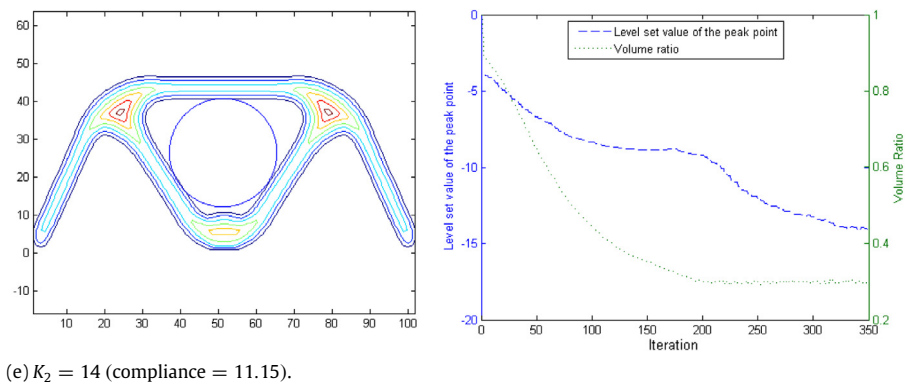
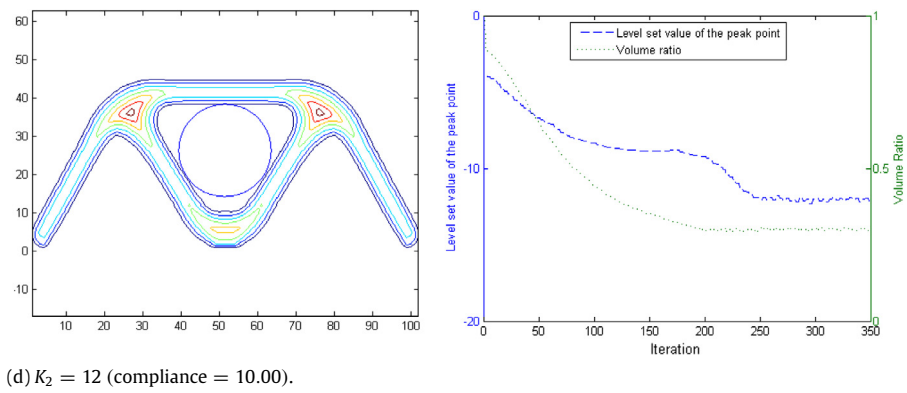
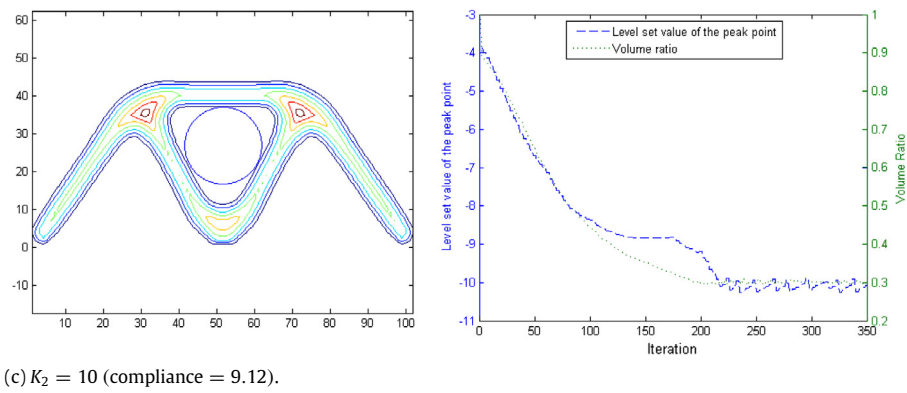
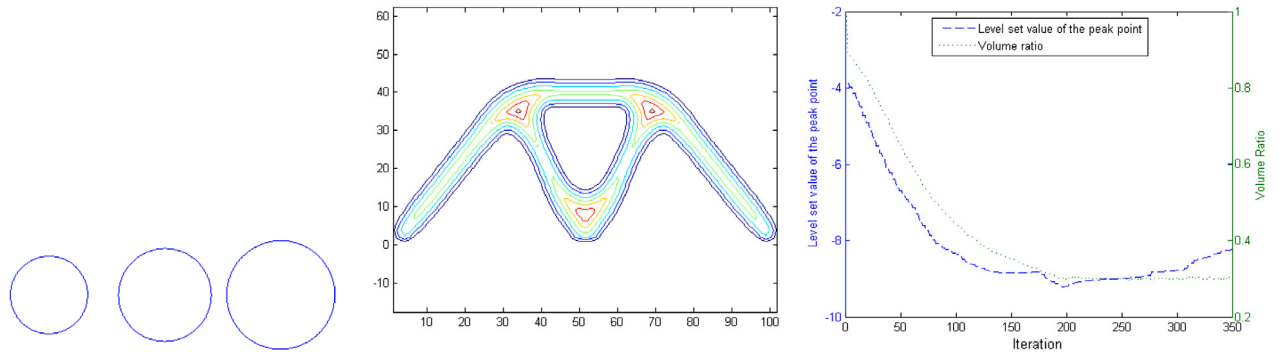


Fig. 4. Topology optimization results and histories under different rough machining lower bounds.

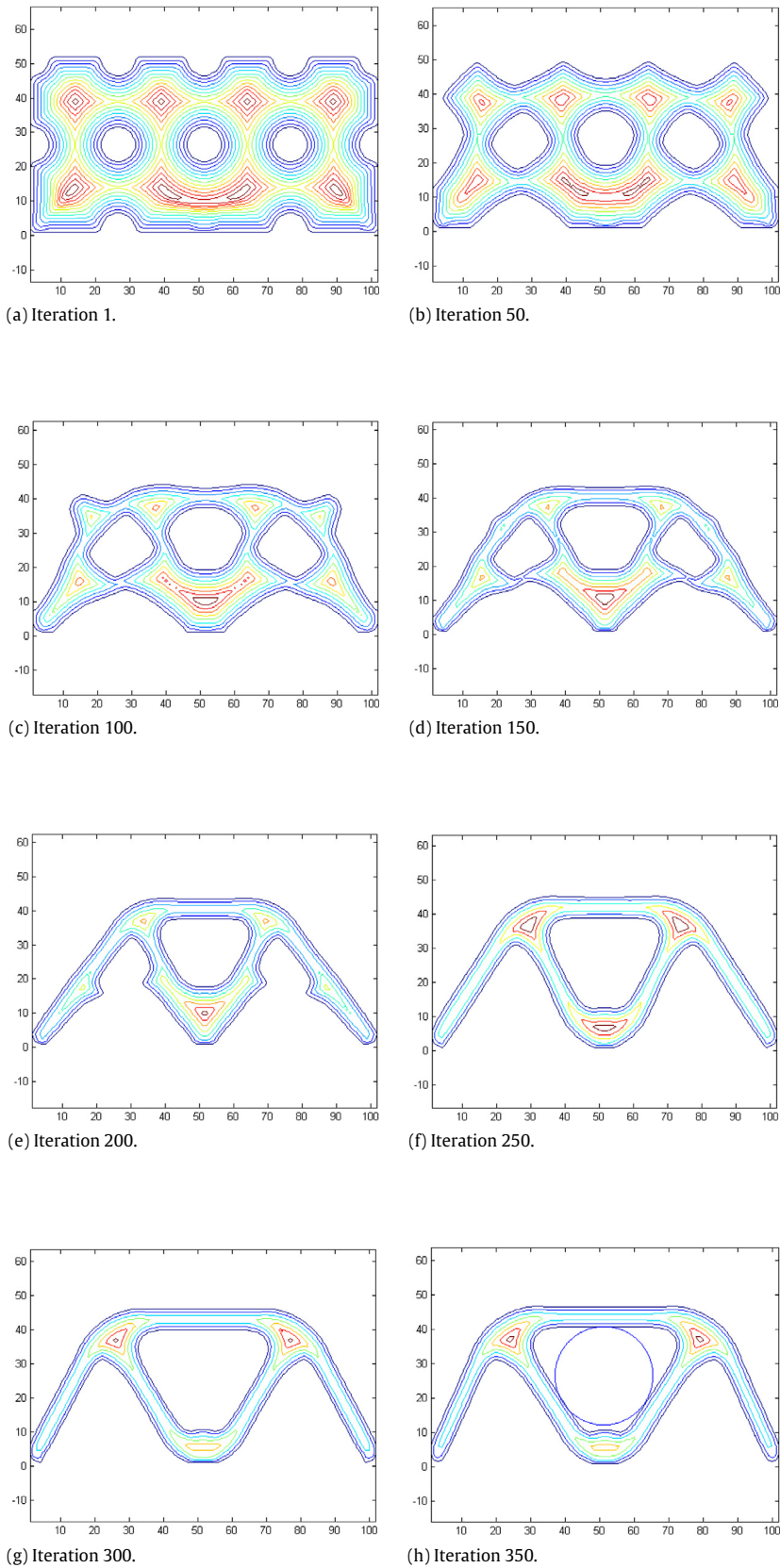


Fig. 5. Entire optimization process under the rough machining lower bound of $K_2 = 14$.



Fig. 6. The cantilever structure problem (100 * 50).

the material volume fraction constraint.

$$\begin{aligned}
 \text{Line 1 : } & \text{Min. } J(\mathbf{u}, \Phi) = \int_D \frac{1}{2} \mathbf{D} \mathbf{e}(\mathbf{u}) \mathbf{e}(\mathbf{u}) H(\Phi) d\Omega \\
 \text{Line 2 : } & \text{s.t. } a(\mathbf{u}, \mathbf{v}, \Phi) = l(\mathbf{v}, \Phi), \quad \forall \mathbf{v} \in U_{ad} \\
 \text{Line 3 : } & \int_D H(\Phi) d\Omega \leq V_{\max} \\
 \text{Line 4 : } & -\frac{1}{R_1} < \kappa(\mathbf{X}) \leq 0, \quad \text{for any } \mathbf{X} \in \partial\Omega^v \text{ or } \partial\Omega^{bv} \\
 \text{Line 5 : } & \kappa = \nabla \cdot \mathbf{n} = \nabla \cdot \left(-\frac{\nabla \Phi(\mathbf{X})}{|\nabla \Phi(\mathbf{X})|} \right) \\
 \text{Line 6 : } & \Phi(P^v_i) \leq -K_2, \quad i = 1, 2, \dots, n \\
 \text{Line 7 : } & a(\mathbf{u}, \mathbf{v}, \Phi) = \int_D \mathbf{D} \mathbf{e}(\mathbf{u}) \mathbf{e}(\mathbf{v}) H(\Phi) d\Omega \\
 \text{Line 8 : } & l(\mathbf{v}, \Phi) = \int_D \mathbf{p} \mathbf{v} H(\Phi) d\Omega \\
 & + \int_D \boldsymbol{\tau} \mathbf{v} \delta(\Phi) |\nabla \Phi| d\Omega.
 \end{aligned} \tag{8}$$

In Eq. (8), line 1 is the objective function, where the structural compliance (sum of the strain energy densities) is to be minimized. Line 2 presents the weak form of the governing equation, where $a(\mathbf{u}, \mathbf{v}, \Phi)$ is the energy bilinear form and $l(\mathbf{v}, \Phi)$ is the load linear form. Specifications of them are demonstrated in lines 7–8. Line 3 shows the material volume fraction constraint. In summary, lines 1–3 and lines 7–8 together form the typical compliance minimization problem subject to the material fraction constraint. For more details, interested readers can refer to [4,5,26]. For the symbols in the problem formulation, \mathbf{u} is the deformation vector, \mathbf{v} is the test vector, and $U_{ad} = \{\mathbf{v} \in H^1(\Omega)^d \mid \mathbf{v} = 0 \text{ on } \Lambda_D\}$ is the space of kinematically admissible displacement field; \mathbf{D} is the elasticity tensor and $\mathbf{e}(\mathbf{u})$ is the strain; V_{\max} is the upper bound of the material volume; $H(\cdot)$ and $\delta(\cdot)$ are the Heaviside function and the Dirac Delta function, which are applied to realize the domain and boundary integrations, respectively.

Other than that, lines 4–6 are the newly added machinability constraints, which have been discussed in the last section. More details about the curvature calculation in line 5 can be found in [53].

About solution of this problem, the Augmented Lagrange Multiplier method is applied and the adjoint sensitivity analysis is performed. Typically, if only considering the compliance-minimization problem but not the void length scale control, the sensitivity analysis result is well known as presented in Eq. (9) [4].

$$\begin{aligned}
 L' &= \int_D R \delta(\Phi) V_n |\nabla \Phi| d\Omega \\
 R &= -\mathbf{D} \mathbf{e}(\mathbf{u}) \mathbf{e}(\mathbf{u}) + \lambda \\
 V_n &= -R.
 \end{aligned} \tag{9}$$

For the constraint in line 6 of Eq. (8), it is not directly solvable because the derived sensitivity result is a local velocity located at the peak point inside the void, which cannot be utilized to

update the zero-value level set contour. Therefore, we switch it into another approximated form as demonstrated in Eq. (10).

$$\begin{aligned}
 V_n(\mathbf{X}) &= -\lambda_i, \quad \mathbf{X} \in \partial\Omega^v_i \\
 \lambda_i^{k+1} &= \max \left(\lambda_i^k + \frac{1}{\mu} (\Phi(P^v_i) + K_2), 0 \right).
 \end{aligned} \tag{10}$$

By utilizing Eq. (10), the entire boundary of the constraint-violating void will uniformly expand. It will be proven in the case study section that, this approximated solution could effectively control the length scale while not evidently affect the proper convergence.

In addition, line 4 in Eq. (8) is also non-trivial in solution through the regular shape sensitivity analysis. Therefore, the curvature flow control technique is applied to address this constraint. Eq. (11) demonstrates the curvature dependent velocities for mean curvature flow control [53], in which b is a positive constant. If $\kappa > 0$, the interface will move in the direction of concavity; and if $\kappa < 0$, the interface will move in the direction of convexity.

$$\mathbf{v} = -b\kappa \mathbf{n}. \tag{11}$$

To satisfy the local curvature constraints, we need to re-define the constant b , that:

$$\begin{aligned}
 b &= 0, \quad \text{if } -\frac{1}{R_1} < \kappa(\mathbf{X}) \leq 0 \\
 b &> 0, \quad \text{if } \kappa(\mathbf{X}) \leq -\frac{1}{R_1} \text{ or } \kappa(\mathbf{X}) > 0.
 \end{aligned} \tag{12}$$

Then, the Hamilton–Jacobi equation is adapted into the convection–diffusion form, which is:

$$\Phi_t + \mathbf{V} \cdot \nabla \Phi = -b\kappa |\nabla \Phi|. \tag{13}$$

5. Numerical examples

In this section, a few numerical examples will be studied to prove the effectiveness of the proposed minimum void length scale control method. All the implementations are based on Matlab.

For all the numerical examples, the finite element analysis (FEA) is performed based on fixed quadrilateral meshes and the artificial weak material is employed for voids in order to avoid the stiffness matrix singularity, which is:

$$\mathbf{D}_v = 10^{-3} \mathbf{D} \tag{14}$$

in which \mathbf{D}_v is the elasticity tensor of the void.

The volume constraint is addressed by the Augmented Lagrange multiplier, as presented in Eq. (15).

$$\begin{aligned}
 \lambda_{k+1} &= \lambda_k + \mu_k \left(\int_D H(\Phi) d\Omega - V_{\max} \right) \\
 \mu_{k+1} &= \alpha \mu_k \quad \text{where } 0 < \alpha < 1
 \end{aligned} \tag{15}$$

in which μ is the penalization factor and α is its adjustment parameter.

5.1. Michell structure design under rough machining lower bound

First, the Michell structure problem is studied only subject to the rough machining lower bound. The boundary condition is shown in Fig. 3, where the two bottom corners are fixed and a vertical unit force is loaded at the bottom middle. The objective is to minimize the structural compliance under the maximum material volume fraction of 0.3. The solid material employs the Young’s Modulus of 1.3 and the Poisson ratio of 0.4.

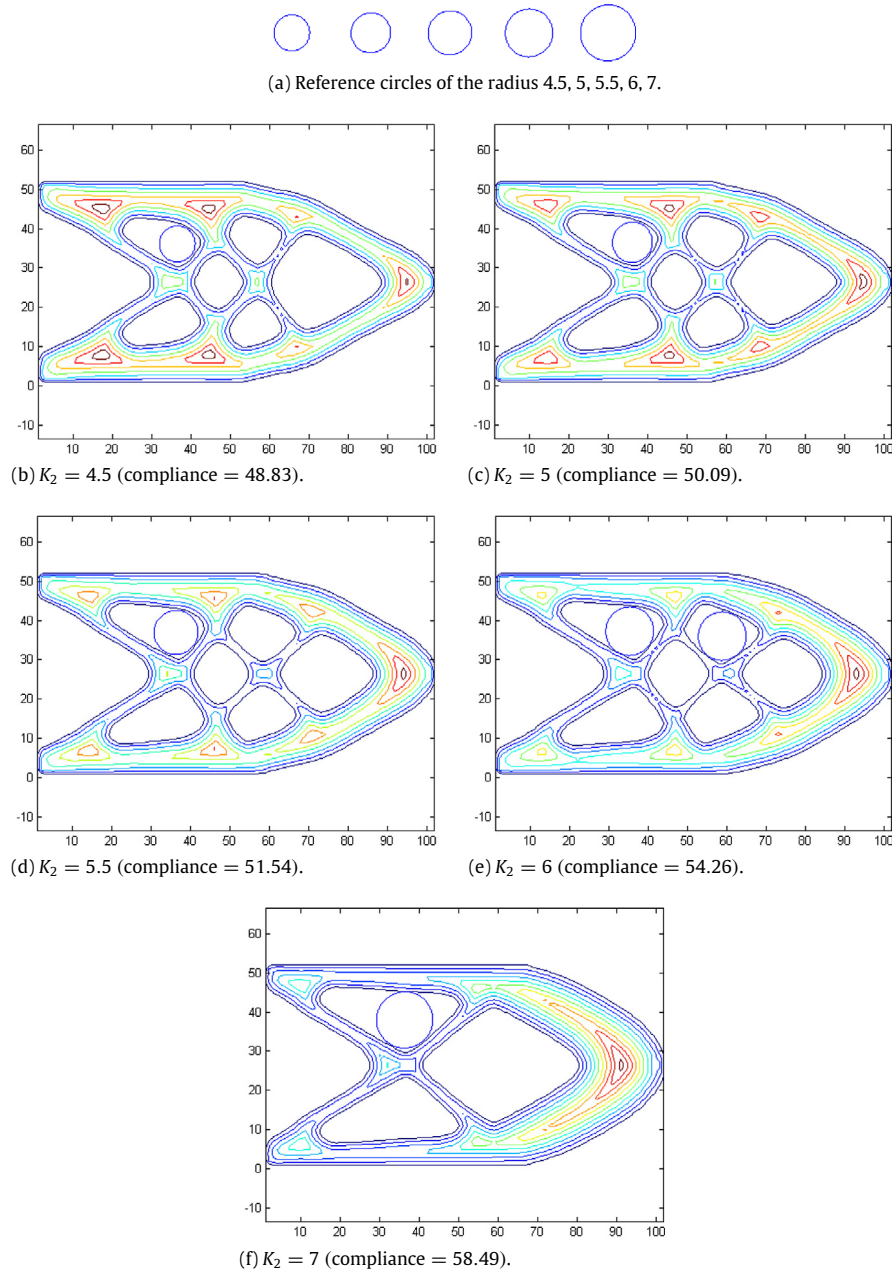


Fig. 7. Topology optimization results under different rough machining lower bounds.

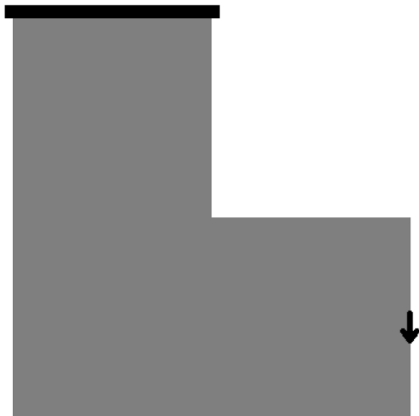
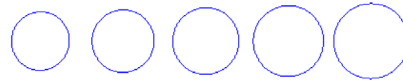


Fig. 8. The L-bracket structure problem (80 * 80).

A set of different rough machining lower bounds are tested, and the related optimization results are demonstrated in Fig. 4. We can see from the results that, (i) the minimum void length scales are well constrained bigger than the different rough machining lower bounds; and (ii) increasing rough machining lower bound slightly sacrifices the structural performance. In addition, the entire optimization process under the rough machining lower bound of $K_2 = 14$ is demonstrated in Fig. 5.

5.2. Cantilever structure design under rough machining lower bounds

Then, the cantilever structure problem is studied subject to different rough machining lower bounds. As shown in Fig. 6, the left side edge is fixed and a vertical unit force is loaded at the middle of the right edge. The objective is to minimize the structural compliance under the maximum material volume



(a) Reference circles of the radius 7, 7.5, 8, 8.5, 9.

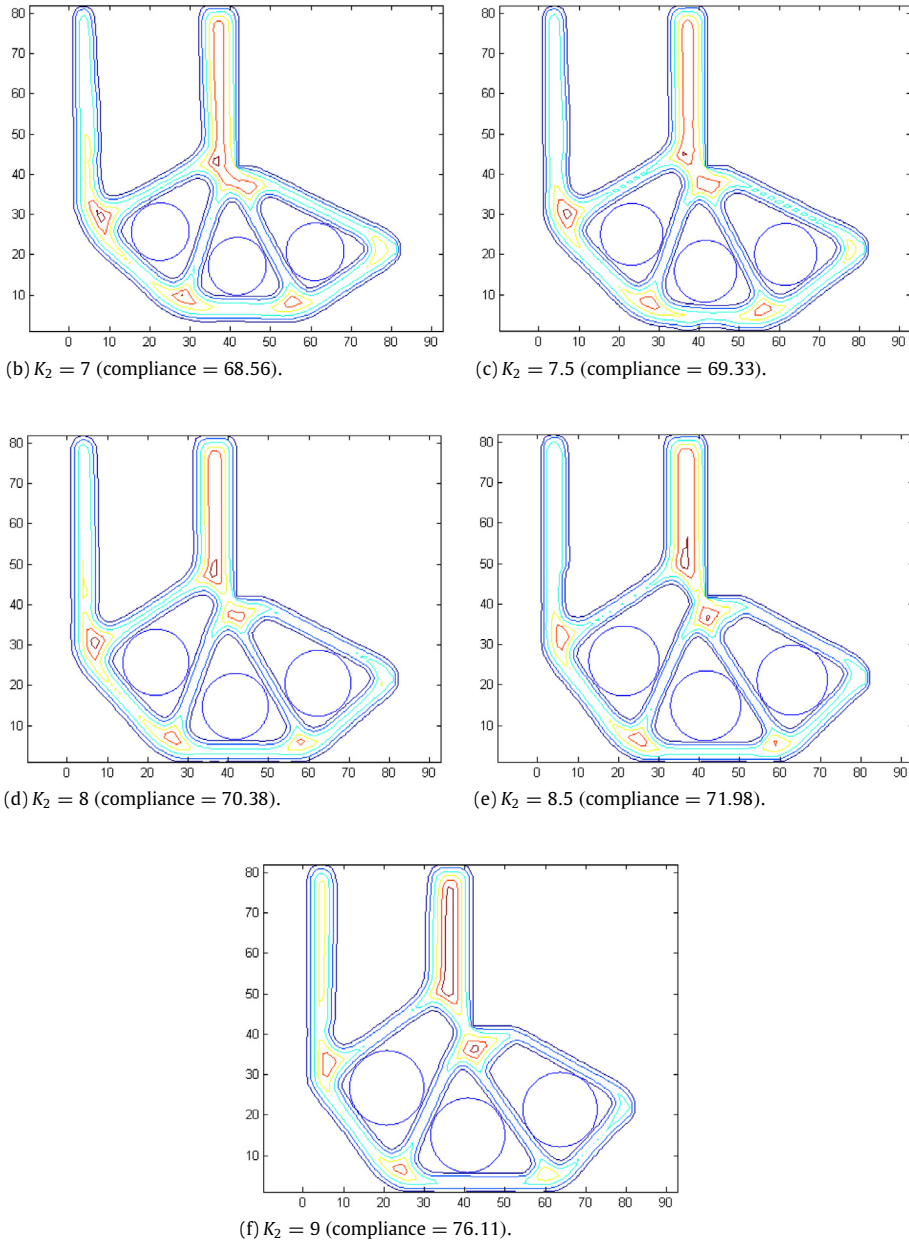


Fig. 9. Topology optimization results under different rough machining lower bounds.

fraction of 0.4. The same material properties used by the last example are employed.

A set of different rough machining lower bounds are tested, and the related optimization results are demonstrated in Fig. 7, from which similar result can be derived as compared to the last example. It is worth noticing that, utilization of a too big rough machining lower bound may break the optimal structural topology; see Fig. 7(f).

5.3. L-bracket structure design under double lower bounds

Then, the L-bracket structure problem is studied subject to both rough and finishing machining lower bounds. As shown in Fig. 8,

the top edge is fixed and a vertical unit force is loaded at the middle of the right edge. The objective is to minimize the structural compliance under the maximum material volume fraction of 0.4. The same material properties used by the last two examples are employed.

A set of different rough machining lower bounds are tested first, and the related optimization results are demonstrated in Fig. 9. Then, the finish machining lower bounds are considered, and the optimization results subject to double lower bounds are presented in Fig. 10. We can see from Figs. 9 and 10 that, sizes of the interior voids (measured by the absolute of the peak point level set value) are always larger than the rough machining lower bounds, i.e. the reference circles are well contained by the interior voids; more

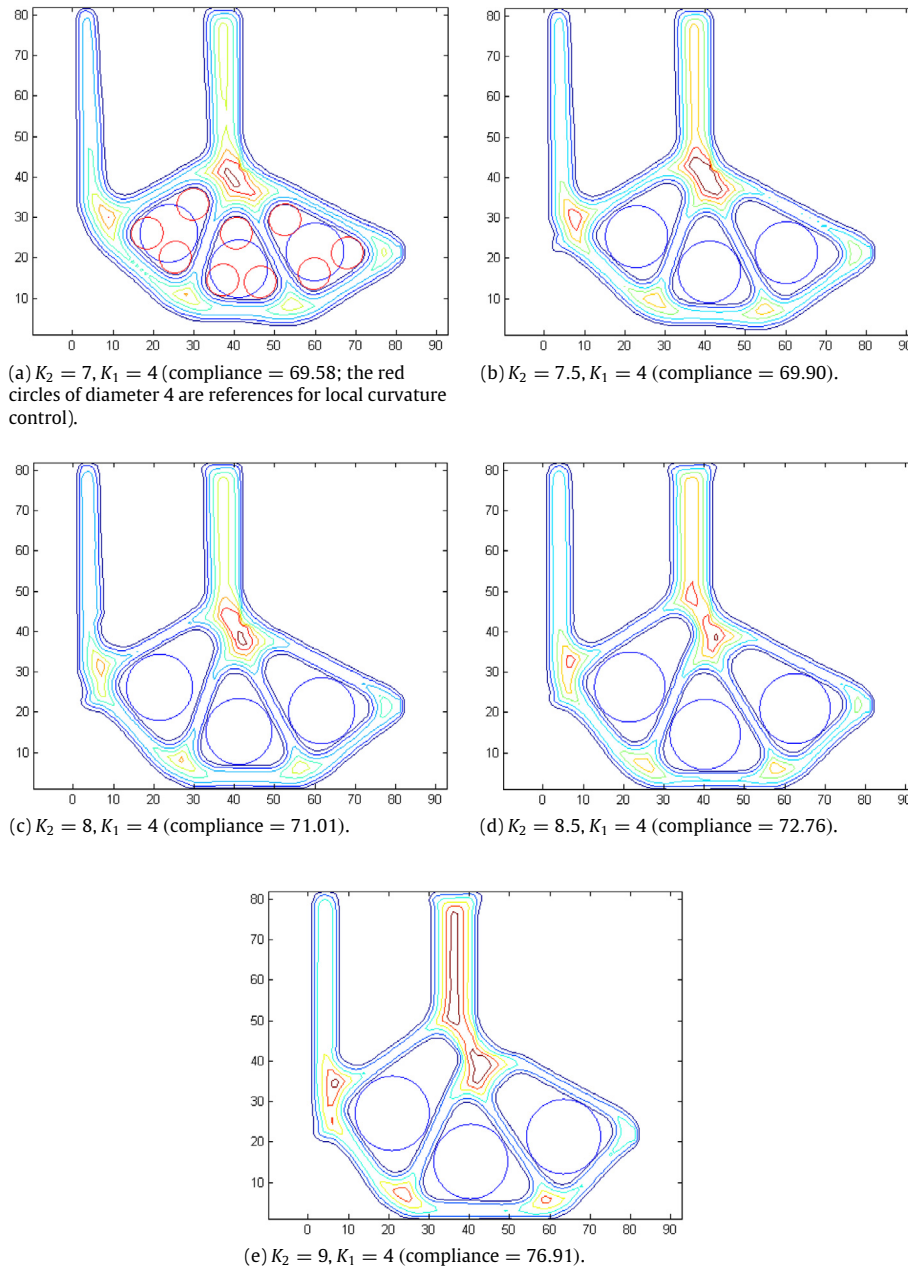


Fig. 10. Topology optimization results under double lower bounds. (For interpretation of the references to color in this figure legend, the reader is referred to the web version of this article.)

importantly, the corner features are well constrained in Fig. 10, by simultaneously applying the finish machining lower bounds, i.e. local radii of the corner features are bigger than the finish machining lower bound K_1 .

5.4. MBB structure design under double lower bounds

The last example is the MBB structure problem, for which both rough and finishing machining lower bounds are applied. As shown in Fig. 11, the two bottom corners are vertically fixed and a vertical unit force is loaded at the middle of the top edge. The objective is to minimize the structural compliance under the maximum material volume fraction of 0.5. The same material properties used by the earlier examples are employed.

A set of different rough machining lower bounds are tested first, and the related optimization results are demonstrated in Fig. 12.



Fig. 11. The L-bracket structure problem (240 * 40).

Then, the finish machining lower bounds are considered, and the optimization results subject to double lower bounds are presented in Fig. 13. From the optimization result, we can draw similar conclusions as compared to the last examples. It is worth noticing that, only the left half of the MBB structure is demonstrated in the results because of the symmetry.

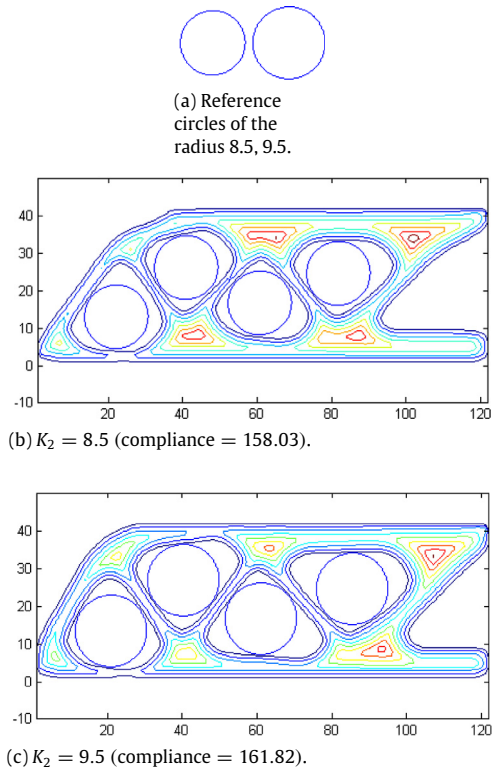


Fig. 12. Topology optimization results under different rough machining lower bounds.

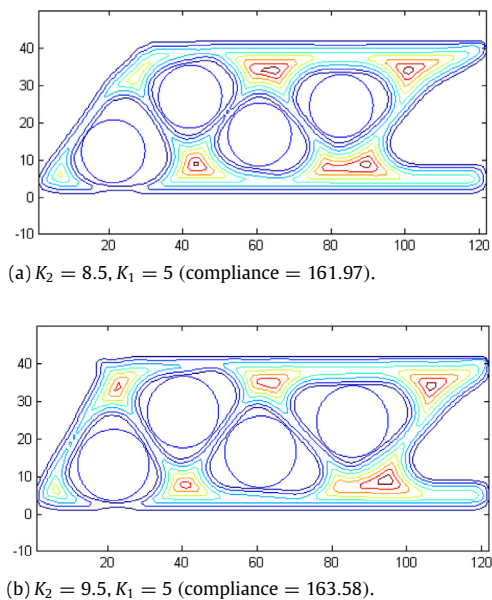


Fig. 13. Topology optimization results under double lower bounds.

In summary of the numerical examples, there is a trade-off between the machining efficiency and the derived structural performance. Generally, by applying a bigger rough machining lower bound, the machining efficiency is better, but the derived structural compliance is bigger as well, which means weaker performance of deformation resistance. Therefore, pursuing better machining efficiency would cause reduced structural performance. Then, if the finish machining lower bound is co-applied, the de-

rived structural compliance would be further sacrificed. Practically, determination of the finish machining lower bound is tightly related to the available cutting tool resources. Hence, the trade-off is necessary to guarantee the parts manufacturable.

6. Conclusion

In this paper, the minimum void length scale control is well addressed under the level set framework. Innovatively, two lower bounds are concurrently applied which correspond to the different machining tool radii of the rough-to-finish machining process. The derived optimal design demonstrates the outstanding characteristics that, both rough and finish machining operations can be effectively performed, through which both the machining efficiency and quality can be guaranteed.

As for the side effects, the applied double lower bounds slightly sacrifice the design optimality. Especially for the rough machining lower bound, if a large value is applied, the optimal structural topology may not be achievable.

For further work, we intent to extend the developed minimum void length scale control method to address stress-constrained problems, which is even more challenging because the stress level is not simply monotonic to the material volume fraction.

Acknowledgments

The authors would like to acknowledge the support from China Scholarship Council (CSC) (2011637036) and Natural Sciences and Engineering Research Council of Canada (NSERC) (RGPIN-2014-05641).

References

- [1] Bendsøe MP, Sigmund O. *Topology optimization*. Berlin, Heidelberg: Springer Berlin, Heidelberg; 2004.
- [2] Xie YM, Steven GP. A simple evolutionary procedure for structural optimization. *Comput & Structures* 1993;49:885–96. [http://dx.doi.org/10.1016/0045-7949\(93\)90035-C](http://dx.doi.org/10.1016/0045-7949(93)90035-C).
- [3] Allaire G, Jouve F, Toader A-M. Structural optimization using sensitivity analysis and a level-set method. *J Comput Phys* 2004;194:363–93. <http://dx.doi.org/10.1016/j.jcp.2003.09.032>.
- [4] Wang MY, Wang X, Guo D. A level set method for structural topology optimization. *Comput Methods Appl Mech Engrg* 2003;192:227–46. [http://dx.doi.org/10.1016/S0045-7825\(02\)00559-5](http://dx.doi.org/10.1016/S0045-7825(02)00559-5).
- [5] Xia Q, Wang MY. Simultaneous optimization of the material properties and the topology of functionally graded structures. *Comput-Aided Des* 2008;40:660–75. <http://dx.doi.org/10.1016/j.cad.2008.01.014>.
- [6] Wei P, Wang MY, Xing XA. study on X-FEM in continuum structural optimization using a level set model. *Comput-Aided Des* 2010;42:708–19. <http://dx.doi.org/10.1016/j.cad.2009.12.001>.
- [7] Borrvall T, Petersson J. Topology optimization of fluids in Stokes flow. *Int J Numer Methods Fluids* 2003;41:77–107. <http://dx.doi.org/10.1002/flid.426>.
- [8] Zhou S, Li Q. A variational level set method for the topology optimization of steady-state Navier–Stokes flow. *J Comput Phys* 2008;227:10178–95. <http://dx.doi.org/10.1016/j.jcp.2008.08.022>.
- [9] Ha S-H, Cho S. Topological shape optimization of heat conduction problems using level set approach. *Numer Heat Transfer B* 2005;48:67–88. <http://dx.doi.org/10.1080/10407790590935966>.
- [10] Yamada T, Izui K, Nishiwaki S. A level set-based topology optimization method for maximizing thermal diffusivity in problems including design-dependent effects. *J Mech Des* 2011;133: <http://dx.doi.org/10.1115/1.4003684>, 031011(9 pages).
- [11] Zhuang C, Xiong Z, Ding H. A level set method for topology optimization of heat conduction problem under multiple load cases. *Comput Methods Appl Mech Engrg* 2007;196:1074–84. <http://dx.doi.org/10.1016/j.cma.2006.08.005>.
- [12] van Dijk NP, Maute K, Langelaar M, van Keulen F. Level-set methods for structural topology optimization: a review. *Struct Multidiscip Optim* 2013;48:437–72. <http://dx.doi.org/10.1007/s00158-013-0912-y>.
- [13] Rozvany GIN. A critical review of established methods of structural topology optimization. *Struct Multidiscip Optim* 2009;37:217–37. <http://dx.doi.org/10.1007/s00158-007-0217-0>.

- [14] Sigmund O, Maute K. Topology optimization approaches. *Struct Multidiscip Optim* 2013;48:1031–55. <http://dx.doi.org/10.1007/s00158-013-0978-6>.
- [15] Guest JK. Topology optimization with multiple phase projection. *Comput Methods Appl Mech Engrg* 2009;199:123–35. <http://dx.doi.org/10.1016/j.cma.2009.09.023>.
- [16] Guest JK. Imposing maximum length scale in topology optimization. *Struct Multidiscip Optim* 2009;37:463–73. <http://dx.doi.org/10.1007/s00158-008-0250-7>.
- [17] Guest JK, Prévost JH, Belytschko T. Achieving minimum length scale in topology optimization using nodal design variables and projection functions. *Internat J Numer Methods Engrg* 2004;61:238–54. <http://dx.doi.org/10.1002/nme.1064>.
- [18] Poulsen TA. A new scheme for imposing a minimum length scale in topology optimization. *Internat J Numer Methods Engrg* 2003;57:741–60. <http://dx.doi.org/10.1002/nme.694>.
- [19] Schevenels M, Lazarov BS, Sigmund O. Robust topology optimization accounting for spatially varying manufacturing errors. *Comput Methods Appl Mech Engrg* 2011;200:3613–27. <http://dx.doi.org/10.1016/j.cma.2011.08.006>.
- [20] Sigmund O. Manufacturing tolerant topology optimization. *Acta Mech Sin* 2009;25:227–39. <http://dx.doi.org/10.1007/s10409-009-0240-z>.
- [21] Sigmund O. Morphology-based black and white filters for topology optimization. *Struct Multidiscip Optim* 2007;33:401–24. <http://dx.doi.org/10.1007/s00158-006-0087-x>.
- [22] Wang F, Lazarov BS, Sigmund O. On projection methods, convergence and robust formulations in topology optimization. *Struct Multidiscip Optim* 2011;43:767–84. <http://dx.doi.org/10.1007/s00158-010-0602-y>.
- [23] Zhang W, Zhong W, Guo X. An explicit length scale control approach in SIMP-based topology optimization. *Comput Methods Appl Mech Engrg* 2014;282:71–86. <http://dx.doi.org/10.1016/j.cma.2014.08.027>.
- [24] Zhou M, Lazarov BS, Wang F, Sigmund O. Minimum length scale in topology optimization by geometric constraints. *Comput Methods Appl Mech Engrg* 2015;293:266–82. <http://dx.doi.org/10.1016/j.cma.2015.05.003>.
- [25] Allaire G, Jouve F, Michailidis G. Thickness control in structural optimization via a level set method. *Struct Multidiscip Optim* 2016;53:1349–82. <http://dx.doi.org/10.1007/s00158-016-1453-y>.
- [26] Chen S, Wang MY, Liu AQ. Shape feature control in structural topology optimization. *Comput-Aided Des* 2008;40:951–62. <http://dx.doi.org/10.1016/j.cad.2008.07.004>.
- [27] Guo X, Zhang W, Zhong W. Explicit feature control in structural topology optimization via level set method. *Comput Methods Appl Mech Engrg* 2014;272:354–78. <http://dx.doi.org/10.1016/j.cma.2014.01.010>.
- [28] Liu J, Ma Y, Fu J, Duke K. A novel CACD/CAD/CAE integrated design framework for fiber-reinforced plastic parts. *Adv Eng Softw* 2015;87:13–29. <http://dx.doi.org/10.1016/j.advengsoft.2015.04.013>.
- [29] Luo J, Luo Z, Chen S, Tong L, Wang MY. A new level set method for systematic design of hinge-free compliant mechanisms. *Comput Methods Appl Mech Engrg* 2008;198:318–31. <http://dx.doi.org/10.1016/j.cma.2008.08.003>.
- [30] Xia Q, Shi T. Constraints of distance from boundary to skeleton: For the control of length scale in level set based structural topology optimization. *Comput Methods Appl Mech Engrg* 2015;295:525–42. <http://dx.doi.org/10.1016/j.cma.2015.07.015>.
- [31] Gersborg AR, Andreassen CS. An explicit parameterization for casting constraints in gradient driven topology optimization. *Struct Multidiscip Optim* 2011;44:875–81. <http://dx.doi.org/10.1007/s00158-011-0632-0>.
- [32] Guest JK, Zhu M. Casting and Milling Restrictions in Topology Optimization via Projection-Based Algorithms, Proceedings of the ASME 2012 International Design Engineering Technical Conference & Computers and Information in Engineering Conference, 2012, 913–920. <http://dx.doi.org/10.1115/DETC2012-71507>.
- [33] Lu J, Chen Y. Manufacturable mechanical part design with constrained topology optimization. *Proc Inst Mech Eng B* 2012;226:1727–35. <http://dx.doi.org/10.1177/0954405412457643>.
- [34] Schramm U, Zhou M. Recent developments in the commercial implementation of topology optimization. In: Bendsøe MP, Olhoff N, Sigmund O, editors. *IUTAM Symp. Topol. Des. Optim. Struct. Mach. Mater.* Netherlands: Springer; 2006. p. 239–48.
- [35] Strömberg N. Topology optimization of structures with manufacturing and unilateral contact constraints by minimizing an adjustable compliance–volume product. *Struct Multidiscip Optim* 2010;42:341–50. <http://dx.doi.org/10.1007/s00158-010-0502-1>.
- [36] Zhou M, Fleury R, Shyy Y-K, Thomas H, Brennan J. Progress in topology optimization with manufacturing constraint, 9th AIAA/ISSMO Symp. Multidiscip. Anal. Optim., 2002.
- [37] Allaire G, Jouve F, Michailidis G. Casting constraints in structural optimization via a level-set method, 2013.
- [38] Liu J, Duke K, Ma Y. Multi-material plastic part design via the level set shape and topology optimization method. *Eng Optim* 2016;48:1910–31. <http://dx.doi.org/10.1080/0305215X.2016.1141203>.
- [39] Xia Q, Shi T, Wang MY, Liu S. A level set based method for the optimization of cast part. *Struct Multidiscip Optim* 2009;41:735–47. <http://dx.doi.org/10.1007/s00158-009-0444-7>.
- [40] Gardan N, Schneider A. Topological optimization of internal patterns and support in additive manufacturing. *J Manuf Syst* 2015;37(Part 1):417–25. <http://dx.doi.org/10.1016/j.jmsy.2014.07.003>.
- [41] Gaynor AT, Meisel NA, Williams CB, Guest JK. Multiple-material topology optimization of compliant mechanisms created via polyjet three-dimensional printing. *J Manuf Sci Eng* 2014;136: <http://dx.doi.org/10.1115/1.4028439>, 061015 (10 pages).
- [42] Meisel N, Williams C. An investigation of key design for additive manufacturing constraints in multimaterial three-dimensional printing. *J Mech Des* 2015;137: <http://dx.doi.org/10.1115/1.4030991>, 111406 (9 pages).
- [43] Zegard T, Paulino GH. Bridging topology optimization and additive manufacturing. *Struct Multidiscip Optim* 2015;53:175–92. <http://dx.doi.org/10.1007/s00158-015-1274-4>.
- [44] Sigmund O. On the design of compliant mechanisms using topology optimization. *Mech Struct Mach* 1997;25:493–524. <http://dx.doi.org/10.1080/08905459708945415>.
- [45] Petersson J, Sigmund O. Slope constrained topology optimization. *Internat J Numer Methods Engrg* 1998;41:1417–34. [http://dx.doi.org/10.1002/\(SICI\)1097-0207\(19980430\)41:8<1417::AID-NME344>3.0.CO;2-N](http://dx.doi.org/10.1002/(SICI)1097-0207(19980430)41:8<1417::AID-NME344>3.0.CO;2-N).
- [46] Sigmund O, Petersson J. Numerical instabilities in topology optimization: A survey on procedures dealing with checkerboards, mesh-dependencies and local minima. *Struct Optim* 1998;16:68–75. <http://dx.doi.org/10.1007/BF01214402>.
- [47] Zuo K-T, Chen L-P, Zhang Y-Q, Yang J. Manufacturing- and machining-based topology optimization. *Int J Adv Manuf Technol* 2005;27:531–6. <http://dx.doi.org/10.1007/s00170-004-2210-8>.
- [48] Wang Y, Zhang L, Wang MY. Length scale control for structural optimization by level sets. *Comput Methods Appl Mech Engrg* 2016;305:891–909. <http://dx.doi.org/10.1016/j.cma.2016.03.037>.
- [49] Liu J, Ma Y. A survey of manufacturing oriented topology optimization methods. *Adv Eng Softw* 2016;100:161–75. <http://dx.doi.org/10.1016/j.advengsoft.2016.07.017>.
- [50] Lazarov BS, Wang F, Sigmund O. Length scale and manufacturability in density-based topology optimization. *Arch Appl Mech* 2016;86:189–218. <http://dx.doi.org/10.1007/s00419-015-1106-4>.
- [51] Shen H, Fu J, Chen Z, Fan Y. Generation of offset surface for tool path in NC machining through level set methods. *Int J Adv Manuf Technol* 2009;46:1043–7. <http://dx.doi.org/10.1007/s00170-009-2164-y>.
- [52] Zhuang C, Xiong Z, Ding H. High speed machining tool path generation for pockets using level sets. *Int J Prod Res* 2010;48:5749–66. <http://dx.doi.org/10.1080/00207540903232771>.
- [53] Osher S, Fedkiw R. *Level set methods and dynamic implicit surfaces*, Vol. 153. New York, NY, New York: Springer; 2003.